

A Comparative Study for the Weighted Nuclear Norm Minimization and Nuclear Norm Minimization

Zhiyuan Zha, Xinggan Zhang, Yu Wu, Qiong Wang and Lan Tang

Abstract—Nuclear norm minimization (NNM) tends to over-shrink the rank components and treats the different rank components equally, thus limits its capability and flexibility. Recent studies have shown that the weighted nuclear norm minimization (WNNM) is expected to be more accurate than NNM. However, it still lacks a plausible mathematical explanation why WNNM is more accurate than NNM. This paper analyzes the WNNM and NNM from the perspective of the group sparse representation (GSR). In particular, an adaptive dictionary for each group is designed to connect the rank minimization and GSR models. Then, we prove that the rank minimization model is equivalent to GSR model. Based on that conclusion, we show mathematically that WNNM is more accurate than NNM. To make the proposed model tractable and robust, the alternative direction multiplier method (ADMM) framework is developed to solve the proposed model. We exploit the proposed scheme to three low level vision tasks, including image deblurring, image inpainting and image compressive sensing (CS) recovery. Experimental results demonstrate that the proposed scheme outperforms many state-of-the-art methods in terms of both quantitative measures and visual perception quality.

Index Terms—WNNM, NNM, GSR, rank minimization, ADMM.

I. INTRODUCTION

Since the data from many practical cases have low rank property in essence, low rank matrix approximation (LRMA), which aims to recover the underlying low rank structure from its degraded/corrupted samples, has a wide range of applications in machine learning and computer vision [1–12]. For instance, the Netflix customer data matrix is regarded as low rank because the customers' choices are mostly affected by a few common factors [5]. The video clip captured by a static camera satisfies the "low rank + sparse" structure so that the background modeling can be conducted by LRMA [7, 8]. As the matrix formed by nonlocal similar patches in a natural image is of low rank, a flurry of matrix completion problems have been proposed, such as collaborative filtering [3], image alignment [9], video denoising [10], shadow removal [11] and reconstruction of occluded/corrupted face images [5].

Generally speaking, methods dealing with LRMA can be classified into two categories: the low rank matrix factorization (LRMF) methods [2, 12] and the nuclear norm (rank)

minimization (NNM) methods [3, 10, 11]. In this work we focus on the latter category. The nuclear norm of a matrix X denoted by $\|X\|_*$, is the sum of its singular values, i.e., $\|X\|_* = \sum_i \sigma_i(X)$, where $\sigma_i(X)$ is the i -th singular value of the matrix X . NNM aims to recover the underlying low rank matrix X from its degraded observation matrix Y , by minimizing $\|X\|_*$. In recent years, a flurry of NNM-based methods have been developed, such as robust principle component analyze (RPCA) [11], background extraction [7], and low rank representation for subspace segmentation [13, 14].

Although NNM has been widely used for low rank matrix approximation, it often ignores the prior knowledge about the singular values of a practical data matrix among which larger ones measure the underlying principle components information. For example, the large singular values of a matrix of image similar patches characterize the major edge and texture information. This means that to recover an image from its degraded/corrupted one, we should shrink larger singular values less and smaller ones more. In a nutshell, NNM is not flexible enough since it treats singular values equally and tends to over-shrink the singular values.

To improve the flexibility of NNM, the weighted nuclear norm minimization (WNNM) model is proposed [15–18]. The weighted nuclear norm of a data matrix X is defined as $\|X\|_{w,*} = \sum_i w_i \sigma_i(X)$, where $w = [w_1, w_2, \dots, w_i]$ and $w_i > 0$ is a non-negative weight assigned to $\sigma_i(X)$. Recent works have demonstrated that WNNM can obtain more accurate results than NNM in various machine learning and computer vision applications [19, 20]. However, mathematically, we are still not clear why WNNM is more accurate than NNM.

With the above consideration, we analyze the WNNM and NNM from the group sparse representation (GSR) perspective. To the best of our knowledge, few works analyze why WNNM is more accurate than NNM mathematically. The contribution of this paper is as follows. First, an adaptive dictionary for each group is designed to connect the rank minimization and GSR models. Second, we prove that the equivalence of rank minimization and GSR models. Based on that conclusion, we show mathematically that WNNM is more accurate than NNM. Third, to make the optimization tractable, we adopt the alternating direction method of multipliers (ADMM) to solve the proposed model. Experimental results on three low-level vision applications, image deblurring, image inpainting and image compressive sensing (CS) recovery, show that the proposed scheme outperforms many state-of-the-art methods both quantitatively and qualitatively.

Z. Zha, X. Zhang, Y. Wu and Q. Wang are with the department of Electronic Science and Engineering, Nanjing University, Nanjing 210023, China. E-mail: zhazhiyuan.mmd@gmail.com.

L. Tang is the department of Electronic Science and Engineering, Nanjing University, and National Mobile Commun. Research Lab., Southeast University, Nanjing 210023, China.

The reminder of this paper is organized as follows. Section II introduces the related work, including group sparse representation (GSR) and the reweighted ℓ_1 norm minimization. Section III analyzes why WNNM is more accurate than NNM, including the related works of NNM and WNNM, an adaptive dictionary for each group is designed to connect the rank minimization and GSR models, and prove the equivalence of the rank minimization and GSR models. Section IV introduces the proposed model in the application of the low level vision tasks and adopts the ADMM method to solve the proposed model. Section V presents the experimental results. Finally, Section VI concludes this paper.

II. RELATED WORK

A. Group Sparse Representation

Traditional patch-based sparse representation assumes that each patch of an image can be precisely encoded as a linear combination of a few atoms selected from a dictionary [21, 22]. It has been successfully used in various image processing and computer vision applications [23, 24]. However, patch-based sparse representation model usually suffers from some limits, such as dictionary learning with great computational complexity and neglecting the correlations between sparsely-coded patches [25–27].

Instead of using patch as the basic unit of sparse representation, group sparse representation (GSR) presents a powerful mechanism, which combines local sparsity and nonlocal self-similarity of images simultaneously in a unified framework [25, 26]. Specifically, an image X with size N is divided into n overlapped patches of size $\sqrt{m} \times \sqrt{m}$, and each patch is denoted by the vector $\mathbf{x}_i \in \mathbb{R}^m, i = 1, 2, \dots, n$. Then for each exemplar patch \mathbf{x}_i , its k similar patches are selected from a $R \times R$ sized search window to form a set \mathcal{S}_i . Since then, all the patches in \mathcal{S}_i are stacked into a data matrix of size $m \times k$, denoted by \mathbf{X}_i , which includes every patch in \mathcal{S}_i as its columns, i.e., $\mathbf{X}_i = \{\mathbf{x}_{i,1}, \mathbf{x}_{i,2}, \dots, \mathbf{x}_{i,k}\}$. The matrix \mathbf{X}_i consisting of all the patches with similar structures is called as a group, where $\mathbf{x}_{i,k}$ denotes the k -th similar patch of the i -th group. Finally, similar to patch-based sparse representation [21, 22], given a dictionary \mathbf{D}_i , each group \mathbf{X}_i can be sparsely represented as $\boldsymbol{\alpha}_i = \mathbf{D}_i^{-1} \mathbf{X}_i$ and solved by the following ℓ_0 -norm minimization problem,

$$\boldsymbol{\alpha}_i = \arg \min_{\boldsymbol{\alpha}_i} \frac{1}{2} \|\mathbf{X}_i - \mathbf{D}_i \boldsymbol{\alpha}_i\|_F^2 + \lambda_i \|\boldsymbol{\alpha}_i\|_0 \quad (1)$$

where $\|\bullet\|_F^2$ denotes the Frobenious norm and λ_i is the regularization parameter. $\|\bullet\|_0$ is ℓ_0 norm, counting the nonzero entries of $\boldsymbol{\alpha}_i$.

However, since the ℓ_0 minimization is discontinuous optimization and NP-hard, solving Eq. (1) is a difficult combinatorial optimization problem. For this reason, it has been suggested that the non-convex ℓ_0 minimization can be replaced by its convex ℓ_1 counterpart,

$$\boldsymbol{\alpha}_i = \arg \min_{\boldsymbol{\alpha}_i} \frac{1}{2} \|\mathbf{X}_i - \mathbf{D}_i \boldsymbol{\alpha}_i\|_F^2 + \lambda_i \|\boldsymbol{\alpha}_i\|_1 \quad (2)$$

Nonetheless, a fact that cannot be ignored is that ℓ_1 minimization is hard to achieve the desired sparsity solution in some practical problems, such as image inverse problems [27].

B. Reweighted ℓ_1 Norm Minimization

To improve the sparsity of ℓ_1 norm, Candès *et al.* [28] proposed the weighted ℓ_1 norm to replace the ℓ_1 norm,

$$\boldsymbol{\alpha}_i = \arg \min_{\boldsymbol{\alpha}_i} \frac{1}{2} \|\mathbf{X}_i - \mathbf{D}_i \boldsymbol{\alpha}_i\|_F^2 + \lambda_i \|\mathbf{w}_i \boldsymbol{\alpha}_i\|_1 \quad (3)$$

where \mathbf{w}_i is the positive weight. Note that, different from ℓ_0 minimization problem in Eq. (1) is non-convex, solving Eq. (3) is a convex optimization problem. Also, the proposition is given as follows,

Proposition 1.

$$\|\mathbf{w}_i \boldsymbol{\alpha}_i\|_1 \succ \|\boldsymbol{\alpha}_i\|_1 \quad (4)$$

where $v_1 \succ v_2$ denotes that the entry v_1 has much more sparsity encouraging than the entry v_2 .

Proof: see [28].

III. WHY WNNM IS MORE ACCURATE THAN NNM

As far as we know, the weighted nuclear norm minimization (WNNM) can achieve more accurate results than nuclear norm minimization (NNM). However, so far, we are still not clear why WNNM is more accurate than NNM because it lacks a feasible mathematical derivation. In this section, we analyze the WNNM and NNM from the group sparse representation (GSR) perspective. First, we introduce the related works of NNM and WNNM. Second, an adaptive dictionary for each group is designed to connect the rank minimization and GSR models. Third, we prove that the equivalence of the rank minimization and GSR models, and thus, we further show mathematically that WNNM is more accurate than NNM.

A. Nuclear Norm Minimization

According to [29], nuclear norm is the tightest convex relaxation of the original rank minimization problem. Given a data matrix $\mathbf{Y} \in \mathbb{R}^{m \times k}$, the goal of NNM is to find a matrix $\mathbf{X} \in \mathbb{R}^{m \times k}$ of rank r , which satisfies the following objective function,

$$\hat{\mathbf{X}} = \arg \min_{\mathbf{X}} \frac{1}{2} \|\mathbf{Y} - \mathbf{X}\|_F^2 + \lambda \|\mathbf{X}\|_* \quad (5)$$

where $\|\mathbf{X}\|_* = \sum_i \sigma_i(\mathbf{X})$, and $\sigma_i(\mathbf{X})$ is the i -th singular value of the matrix \mathbf{X} . λ is a positive constant. Candès *et al.* [30] showed that the low rank matrix can be perfectly recovered from the degraded/corrupted data matrix with high probability by solving an NNM problem. Cai *et al.* [3] proved that NNM problem can be easily solved by imposing a soft-thresholding operation, that is, the solution of Eq. (5) which can be solved by

$$\hat{\mathbf{X}} = \mathbf{U} \mathbf{S}_\lambda(\boldsymbol{\Sigma}) \mathbf{V}^T \quad (6)$$

where $\mathbf{Y} = \mathbf{U} \boldsymbol{\Sigma} \mathbf{V}^T$ is the SVD of \mathbf{Y} and $\mathbf{S}_\lambda(\boldsymbol{\Sigma})$ is the soft-thresholding operator function on diagonal matrix $\boldsymbol{\Sigma}$ with parameter λ . For each diagonal element Σ_{ii} in $\boldsymbol{\Sigma}$, there is $\mathbf{S}_\lambda(\boldsymbol{\Sigma})_{ii} = \text{soft}(\Sigma_{ii}, \lambda) = \max(\Sigma_{ii} - \lambda, 0)$.

More Specifically, they proved the following theorem.

Theorem 1. For each $\lambda \geq 0$ and \mathbf{Y} , the singular value shrinkage operator Eq. (6) obeys Eq. (5).

Proof: see [3].

B. Weighted Nuclear Norm Minimization

As an alternative, the weighted nuclear norm minimization (WNNM) model is proposed [15–18]. That is, the weighted nuclear norm $\|X\|_{w,*}$ used to regularize X and Eq. (5) can be rewritten as

$$\hat{X} = \arg \min_X \frac{1}{2} \|Y - X\|_F^2 + \|X\|_{w,*} \quad (7)$$

where $\|X\|_{w,*} = \sum_i w_i \sigma_i(X)$, $w = [w_1, w_2, \dots, w_i]$ and $w_i > 0$ is a non-negative weight assigned to $\sigma_i(X)$. Also, Gu *et al.* [15] proved the following theorem.

Theorem 2. *If the singular values $\sigma_1 \geq \dots \geq \sigma_{n_0}$ and the weights satisfy $0 \leq w_1 \leq \dots \leq w_{n_0}$, $n_0 = \min(m, k)$, the WNNM problem in Eq. (7) has a globally optimal solution*

$$\hat{X} = US_w(\Sigma)V^T \quad (8)$$

where $Y = U\Sigma V^T$ is the SVD of Y and $S_w(\Sigma)$ is the generalized soft-thresholding operator with the weighted vector w , i.e., $S_w(\Sigma)_{ii} = \text{soft}(\Sigma_{ii}, w_i) = \max(\Sigma_{ii} - w_i, 0)$.

Proof: see [15].

To prove that WNNM is more accurate than NNM, we have the following theorem.

Theorem 3. *For $0 \leq w_1 \leq \dots \leq w_{n_0}$ and Y , $n_0 = \min(m, k)$, the singular value shrinkage operator Eq. (8) satisfies Eq. (7).*

The detailed proof of the Theorem 3 is given in the Appendix A.

Note that the relationship between Theorem 3 is the necessary and sufficient condition of Theorem 2.

C. Adaptive Dictionary Learning

In this subsection, an adaptive dictionary learning approach is designed. To be concrete, for each group X_i , its adaptive dictionary can be learned from its observation $Y_i \in \mathbb{R}^{m \times k}$.

Then, we apply the singular value decomposition (SVD) to Y_i ,

$$Y_i = U_i \Sigma_i V_i^T = \sum_{j=1}^{n_0} \sigma_{i,j} u_{i,j} v_{i,j}^T \quad (9)$$

where $\mu_i = [\sigma_{i,1}, \sigma_{i,2}, \dots, \sigma_{i,n_0}]$, $n_0 = \min(m, k)$, $\Sigma_i = \text{diag}(\mu_i)$ is a diagonal matrix whose non-zero elements are represented by μ_i , and $u_{i,j}, v_{i,j}$ are the columns of U_i and V_i , respectively.

Moreover, we define each dictionary atom $d_{i,j}$ of the adaptive dictionary D_i for each group Y_i as follows:

$$d_{i,j} = u_{i,j} v_{i,j}^T, \quad j = 1, 2, \dots, n_0 \quad (10)$$

Finally, learning an adaptive dictionary from each group Y_i can be constructed by $D_i = [d_{i,1}, d_{i,2}, \dots, d_{i,n_0}]$. The proposed dictionary learning approach is efficient due to the fact that it only requires one SVD operator for each group.

D. WNNM is More Accurate than NNM

To prove that WNNM is more accurate than NNM, we need the following lemmas:

Lemma 1. *The minimization problem*

$$x = \arg \min_x \frac{1}{2} \|x - a\|_2^2 + \tau \|x\|_1 \quad (11)$$

has a closed-form solution, which can be expressed as

$$\hat{x} = \text{soft}(a, \tau) = \text{sgn}(a, \tau) \cdot \max(\text{abs}(a) - \tau, 0) \quad (12)$$

Proof: see [31].

Lemma 2. *For the following optimization problem*

$$\min_{x_i \geq 0} \frac{1}{2} \sum_{i=1}^n (x_i - a_i)^2 + w_i x_i \quad (13)$$

If $a_1 \geq \dots \geq a_n \geq 0$ and the weights satisfy $0 \leq w_1 \leq \dots \leq w_n$, then the global optimum of Eq. (13) is $\hat{x}_i = \text{soft}(a_i, w_i) = \max(a_i - w_i, 0)$.

The detailed proof of the Lemma 2 can be found in the Appendix B.

Now, the ℓ_1 norm-based group sparse representation problem can be expressed in Eq. (2). According to the above design of adaptive dictionary D_i in Eq. (10), we have the following theorem.

Theorem 4.

$$\|Y_i - X_i\|_F^2 = \|\mu_i - \alpha_i\|_2^2 \quad (14)$$

where $Y_i = D_i \mu_i$ and $X_i = D_i \alpha_i$.

The detailed proof of the Theorem 4 is given in the Appendix C.

Therefore, based on the Proposition 2, Lemma (1, 2) and Theorem (1, 2, 3, 4), we can prove that

Proposition 2. *WNNM is more accurate than NNM under the adaptive dictionary D_i .*

The detailed proof of the Proposition 2 is given in the Appendix D.

Note that the main difference between sparse representation model and the rank minimization model is that sparse representation model has a dictionary learning operator and the rank minimization model does not involve.

IV. GROUP-BASED SPARSE REPRESENTATION FOR LOW LEVEL VISION TASKS VIA THE WEIGHTED ℓ_1 MINIMIZATION

In this section, we demonstrate the proposed scheme in the application of the low level vision tasks, including image deblurring, image inpainting and image compressive sensing (CS) recovery. The goal of the low level vision tasks is to reconstruct a high quality image X from its degraded observation Y , which is a typical ill-posed inverse problem and can be mathematically expressed as

$$Y = HX + \varphi \quad (15)$$

where X, Y denote the original image and the degraded image, respectively. H is the degraded operator and φ is usually assumed to be additive white Gaussian noise.

In the scenario of the low level vision tasks, what we observed is the degraded image Y in Eq. (15), and thus we utilize GSR model to reconstruct X from Y by solving the following weighted ℓ_1 minimization problem,

$$\alpha = \arg \min_{\alpha} \frac{1}{2} \|Y - H\alpha\|_2^2 + \lambda \|\alpha\|_1 \quad (16)$$

where λ is a regularization parameter.

The problem in Eq. (16) can be solved by the iterative shrinkage (IST) algorithm [32]. However, the major drawback of the IST algorithm is its low convergence speed. In this paper, we adopt the algorithm framework of the alternating direction method of multipliers (ADMM) [33] to solve Eq. (16).

ADMM method is a powerful tool for various large scale optimization problems and its basic idea is to translate the unconstrained minimization problem into a constrained one by variable splitting. Numerical simulations have demonstrated that it can converge by only using a small memory footprint, which makes it very attractive for numerous large-scale optimization problems [34–36]. We will briefly introduce ADMM through considering a constrained optimization,

$$\min_{\mathbf{u} \in \mathbb{R}^N, \mathbf{a} \in \mathbb{R}^M} f(\mathbf{u}) + g(\mathbf{a}), \quad s.t. \quad \mathbf{u} = \mathbf{G}\mathbf{a} \quad (17)$$

where $\mathbf{G} \in \mathbb{R}^{M \times N}$ and $f : \mathbb{R}^N \rightarrow \mathbb{R}$, $g : \mathbb{R}^M \rightarrow \mathbb{R}$. The ADMM works as follows:

Algorithm 1 ADMM Method.

1. **Initialization** t , choose $\rho > 0$, \mathbf{u} , \mathbf{a} , and \mathbf{C} .
2. **Repeat**
3. $\mathbf{u}^{t+1} = \arg \min_{\mathbf{u}} f(\mathbf{u}) + \frac{\rho}{2} \|\mathbf{u} - \mathbf{G}\mathbf{a}^t - \mathbf{C}^t\|_2^2$;
4. $\mathbf{a}^{t+1} = \arg \min_{\mathbf{a}} g(\mathbf{a}) + \frac{\rho}{2} \|\mathbf{u}^{t+1} - \mathbf{G}\mathbf{a} - \mathbf{C}^t\|_2^2$;
5. $\mathbf{C}^{t+1} = \mathbf{C}^t - (\mathbf{u}^{t+1} - \mathbf{G}\mathbf{a}^{t+1})$;
6. $t \leftarrow t + 1$;
7. **Until** stopping criterion is satisfied.

Now, we introduce an auxiliary variable \mathbf{U} and Eq. (16) can be rewritten as

$$\alpha = \arg \min_{\mathbf{U}, \alpha} \frac{1}{2} \|\mathbf{Y} - \mathbf{H}\mathbf{U}\|_2^2 + \lambda \|\mathbf{w}\alpha\|_1, \quad s.t. \quad \mathbf{U} = \mathbf{D}\alpha \quad (18)$$

By defining $f(\mathbf{U}) = \frac{1}{2} \|\mathbf{Y} - \mathbf{H}\mathbf{U}\|_2^2$, and $g(\alpha) = \lambda \|\mathbf{w}\alpha\|_1$, we have

$$\mathbf{U}^{t+1} = \arg \min_{\mathbf{U}} \frac{1}{2} \|\mathbf{Y} - \mathbf{H}\mathbf{U}\|_2^2 + \frac{\rho}{2} \|\mathbf{U} - \mathbf{D}\alpha^t - \mathbf{C}^t\|_2^2 \quad (19)$$

$$\alpha^{t+1} = \arg \min_{\alpha} \lambda \|\mathbf{w}\alpha\|_1 + \frac{\rho}{2} \|\mathbf{U}^{t+1} - \mathbf{D}\alpha - \mathbf{C}^t\|_2^2 \quad (20)$$

and

$$\mathbf{C}^{t+1} = \mathbf{C}^t - (\mathbf{U}^{t+1} - \mathbf{D}\alpha^{t+1}) \quad (21)$$

It can be seen that the minimization for Eq. (16) involves splitting two minimization sub-problems, i.e., \mathbf{U} and α sub-problems. Next, we will show that there is an efficient solution to each sub-problem. To avoid confusion, the subscribe t may be omitted for conciseness.

A. Subproblem of Minimizing \mathbf{U} for fixed α

Given α , the \mathbf{U} sub-problem denoted by Eq. (19) becomes

$$\min_{\mathbf{U}} \mathcal{Q}_1(\mathbf{U}) = \min_{\mathbf{U}} \frac{1}{2} \|\mathbf{Y} - \mathbf{H}\mathbf{U}\|_2^2 + \frac{\rho}{2} \|\mathbf{U} - \mathbf{D}\alpha - \mathbf{C}\|_2^2 \quad (22)$$

Clearly, Eq. (22) has a closed-form solution and its solution can be expressed as

$$\hat{\mathbf{U}} = (\mathbf{H}^T \mathbf{H} + \rho \mathbf{I})^{-1} (\mathbf{H}^T \mathbf{Y} + \rho (\mathbf{D}\alpha + \mathbf{C})) \quad (23)$$

where \mathbf{I} represents the identity matrix.

Due to the specific structure of \mathbf{H} in image deblurring and image inpainting, Eq. (23) can be efficiently computed without matrix inversion (more details can be seen in [37]).

However, \mathbf{A} is a random projection matrix without a special structure in image CS recovery, computing the inverse by Eq. (23) at each iteration is too costly to implement numerically. Therefore, to avoid computing the matrix inversion, an iterative algorithm is highly desired for solving Eq. (22). This work adopts the gradient descent method [38] with an optimal step to solve Eq. (22), i.e.,

$$\hat{\mathbf{U}} = \mathbf{U} - \eta \mathbf{q} \quad (24)$$

where \mathbf{q} is the gradient direction of the objective function $\mathcal{Q}_1(\mathbf{U})$, and η is the optimal step.

Thus, in image CS recovery, it only requires an iterative calculation of the following equation to solve the \mathbf{U} sub-problem,

$$\hat{\mathbf{U}} = \mathbf{U} - \eta (\mathbf{H}^T \mathbf{H} \mathbf{U} - \mathbf{H}^T \mathbf{Y} + \rho (\mathbf{U} - \mathbf{D}\alpha - \mathbf{C})) \quad (25)$$

where $\mathbf{H}^T \mathbf{H}$ and $\mathbf{H}^T \mathbf{Y}$ can be calculated in advance.

B. Subproblem of Minimizing α for fixed \mathbf{U}

Given \mathbf{U} , similarly, according to Eq. (20), the α sub-problem can be written as

$$\min_{\alpha} \mathcal{Q}_2(\alpha) = \min_{\alpha} \frac{1}{2} \|\mathbf{D}\alpha - \mathbf{L}\|_2^2 + \frac{\lambda}{\rho} \|\mathbf{w}\alpha\|_1 \quad (26)$$

where $\mathbf{L} = \mathbf{U} - \mathbf{C}$. However, due to the complex definition of $\|\mathbf{w}\alpha\|_1$, it is difficult to solve Eq. (26) directly. Let $\mathbf{X} = \mathbf{D}\alpha$, Eq. (26) can be rewritten as

$$\min_{\alpha} \mathcal{Q}_2(\alpha) = \min_{\alpha} \frac{1}{2} \|\mathbf{X} - \mathbf{L}\|_2^2 + \frac{\lambda}{\rho} \|\mathbf{w}\alpha\|_1 \quad (27)$$

To make Eq. (27) tractable, a general assumption is made, with which even a closed-form solution of Eq. (27) can be achieved. More specifically, \mathbf{L} can be regarded as some type of noisy observation of \mathbf{X} , and thus $\mathbf{R} = \mathbf{X} - \mathbf{L}$ follows an independent zero mean distribution with variances δ^2 . The following theorem can be proven with this assumption.

Theorem 5. Defining $\mathbf{X}, \mathbf{L} \in \mathbb{R}^N$, $\mathbf{X}_i, \mathbf{L}_i \in \mathbb{R}^{m \times k}$, and $\mathbf{e}(j)$ as each element of error vector \mathbf{e} , where $\mathbf{e} = \mathbf{X} - \mathbf{L}$, $j = 1, \dots, N$. Assume that $\mathbf{e}(j)$ follows an independent zero mean distribution with variance δ^2 , and thus for any $\varepsilon > 0$, we can represent the relationship between $\frac{1}{N} \|\mathbf{X} - \mathbf{L}\|_2^2$ and $\frac{1}{K} \sum_{i=1}^n \|\mathbf{X}_i - \mathbf{L}_i\|_2^2$ by the following property,

$$\lim_{\substack{N \rightarrow \infty \\ K \rightarrow \infty}} \mathbf{P}\left\{ \left| \frac{1}{N} \|\mathbf{X} - \mathbf{L}\|_2^2 - \frac{1}{K} \sum_{i=1}^n \|\mathbf{X}_i - \mathbf{L}_i\|_2^2 \right| < \varepsilon \right\} = 1 \quad (28)$$

where $\mathbf{P}(\bullet)$ represents the probability and $K = m \times k \times n$.

The detailed proof of the Theorem 5 is given in the Appendix E.

Thus, based on Theorem 5, we have the following equation with a very large probability (restricted 1) at each iteration,

$$\frac{1}{N} \|\mathbf{X} - \mathbf{L}\|_2^2 = \frac{1}{K} \sum_{i=1}^n \|\mathbf{X}_i - \mathbf{L}_i\|_2^2 \quad (29)$$

And thus, Eq. (27) can be rewritten as

$$\begin{aligned} & \min_{\alpha} \frac{1}{2} \|X - L\|_2^2 + \frac{\lambda}{\rho} \|w\alpha\|_1 \\ & = \min_{\alpha_i} \left(\sum_{i=1}^n \frac{1}{2} \|X_i - L_i\|_F^2 + \tau_i \|w_i \alpha_i\|_1 \right) \quad (30) \\ & = \min_{\alpha_i} \left(\sum_{i=1}^n \frac{1}{2} \|L_i - D_i \alpha_i\|_F^2 + \tau_i \|w_i \alpha_i\|_1 \right) \end{aligned}$$

where $\tau_i = \lambda_i K / \rho N$ and D_i is a dictionary. It can be seen that Eq. (30) can be regarded as a group sparse representation problem by solving n sub-problems for all the group X_i . Based on Theorem 4, Eq. (30) can be rewritten as

$$\hat{\alpha}_i = \min_{\alpha_i} \sum_{i=1}^n \frac{1}{2} \|\gamma_i - \alpha_i\|_2^2 + \tau_i \|w_i \alpha_i\|_1 \quad (31)$$

where $L_i = D_i \gamma_i$ and $X_i = D_i \alpha_i$. Therefore, based on Lemma 2, a closed-form solution of Eq. (31) can be computed as

$$\hat{\alpha}_i = \text{soft}(\gamma_i, \tau_i w_i) = \max(\text{abs}(\gamma_i) - \tau_i w_i, 0) \quad (32)$$

For each weight w_i , large values of sparse coefficient α_i usually transmit major edge and texture information. This implies that to reconstruct X_i from its degraded one, we should shrink large values less, while shrinking smaller ones more. Therefore, we let

$$w_i = \frac{1}{|\gamma_i| + \epsilon} \quad (33)$$

where ϵ is a small constant.

The parameter λ that balances the fidelity term and the regularization term should be adaptively determined for better reconstruction performance. In this paper, inspired by [39], the regularization parameter λ_i of each group L_i is set as:

$$\lambda_i = \frac{2\sqrt{2}\delta^2}{\theta_i + \varrho} \quad (34)$$

where θ_i denotes the estimated variance of γ_i , and ϱ is a small constant.

After solving the two sub-problems, we summarize the overall algorithm for Eq. (16) in Table I.

V. EXPERIMENTAL RESULTS



Fig. 1. All test images. Top: Cowboy, Light, Barbara, boats, rampart, House, Granny, Cruzcampo. Middle: Mickey, billboard, Flower, plants, Monk, Fence, building, castle. Below: Swamm, Leaves, Corner, foreman, straw, Girl, Monarch, clock.

In this section, we report our experimental results in the applications of image deblurring, image inpainting and image CS recovery. All the experimental images are shown in Fig.1.

TABLE I
ADMM METHOD FOR THE PROPOSED MODEL.

Input:	the observed image Y and the measurement matrix H .
Initialization:	$C, U, \alpha, R, m, k, \rho, \delta, \epsilon, \varrho, t$;
Repeat	
If H is blur operator or mask operator	Update U^{t+1} by Eq. (23);
Else H is random projection operator	Update U^{t+1} Eq. (25);
End if	
$L^{t+1} = U^{t+1} - C^t$;	
For	Each group L_i ;
Construct dictionary D_i by computing Eq. (10);	
Update λ_i^{t+1} by computing Eq. (34);	
Update τ_i^{t+1} computing by $\tau_i = \lambda_i K / \rho N$;	
Update w_i^{t+1} computing by Eq. (33);	
Update α_i^{t+1} computing by Eq. (32);	
End For	
Update D^{t+1} by concatenating all D_i ;	
Update α^{t+1} by concatenating all α_i ;	
Update C^{t+1} by computing Eq. (21) ;	
$t \leftarrow t + 1$;	
Until	maximum iteration number is reached.
Output:	The final restored image $\hat{X} = D\hat{\alpha}$.

Since the group sparse representation (GSR) is exploited to prove that WNNM is more accurate than NNM, we called the proposed scheme as GSR-WNNM. To verify the effectiveness of WNNM, we have implemented a variant of the GSR that use NNM, denoted as GSR-NNM. To evaluate the quality of the restored images, the PSNR and the recently proposed powerful perceptual quality metric FSIM [40] are calculated.

A. Image Deblurring

In this subsection, we have compared the proposed GSR-WNNM with five other competing approaches: IDD-BM3D [41], NCSR [42], FPD [43], MSEPLL [44] and GSR-NNM. Note that IDD-BM3D and NCSR are the recently developed state-of-the-art non-blind image deblurring methods. In our comparative study, three blur kernels, 9×9 uniform kernel, a Gaussian kernel (fspecial('gaussian', 25, 1.6)) and a motion kernel (fspecial('motion', 20, 45)) are used. Blurred images are further corrupted by additive white Gaussian noise with $\delta = 2$. The parameters are set as follows. The size of searching window $R \times R$ is set to be 40×40 and searching matched patches $k = 60$. The size of each patch $\sqrt{m} \times \sqrt{m}$ is set to be 8×8 . We assign $\varrho = 0.1$ and $\epsilon = 0.35$. $\rho = 0.0225, 0.0225$ and 0.0375 for uniform, Gaussian and motion kernel, respectively.

Table II lists the PSNR comparison results for a collection of 8 images among five competing methods. It can be seen that GSR-WNNM outperforms other methods for all three types of blur kernels. The visual comparisons of the deblurring methods are shown in Fig. 2 and Fig. 3, respectively. One can observe that NCSR, FPD, MSEPLL and GSR-NNM still generate some undesirable artifacts, while IDD-BM3D results in over-smooth phenomena. By contrast, GSR-WNNM is able to preserve the sharpness of edges and suppress undesirable artifacts more effectively than other competing methods.

TABLE II
PSNR (dB) COMPARISONS FOR IMAGE DEBLURRING.

Images	billboard	Cruzcampo	rampart	Corner	Barbara	castle	building	clock
9 × 9 Uniform Kernel, $\delta = 2$								
IDD-BM3D [41]	23.23	26.12	25.46	24.26	26.31	25.97	21.63	26.53
NCSR [42]	23.29	26.23	25.59	24.42	26.28	26.00	21.36	26.50
FPD [43]	22.34	25.29	25.28	23.18	24.66	25.27	20.14	26.00
MSEPLL [44]	22.88	25.67	25.22	23.79	25.63	25.33	21.22	25.56
GSR-NNM	22.35	25.17	24.98	23.50	25.82	25.23	20.81	25.30
GSR-WNNM	23.69	26.65	25.85	24.74	26.82	26.30	21.69	27.09
Gaussian Kernel : fspecial('gaussian', 25, 1.6), $\delta = 2$								
IDD-BM3D [41]	23.67	25.72	25.99	25.13	25.00	26.83	20.62	28.11
NCSR [42]	23.67	25.65	26.08	25.22	24.90	26.86	20.62	28.23
FPD [43]	23.50	25.80	25.98	25.03	24.41	26.77	20.56	28.13
MSEPLL [44]	23.63	25.89	25.81	25.11	24.21	26.60	20.57	28.01
GSR-NNM	22.90	25.01	25.37	24.58	24.24	26.30	20.34	27.18
GSR-WNNM	23.87	25.91	26.16	25.35	25.71	26.99	20.64	28.45
Motion Kernel : fspecial('motion', 20, 45), $\delta = 2$								
IDD-BM3D [41]	25.46	26.54	26.18	25.49	27.55	26.58	21.32	28.04
NCSR [42]	25.47	26.45	26.21	24.55	27.38	25.90	20.59	27.15
FPD [43]	23.72	25.74	26.10	23.18	24.66	25.27	19.94	26.00
MSEPLL [44]	24.94	25.89	25.62	24.34	25.52	25.71	20.96	26.69
GSR-NNM	23.95	25.11	25.22	24.49	26.28	25.67	20.48	26.80
GSR-WNNM	26.16	27.03	27.19	26.33	29.07	27.25	21.44	28.87



Fig. 2. Deblurring performance comparison on the *Barbara* image. (a) Original image; (b) Noisy and blurred image (fspecial('gaussian', 25, 1.6), $\delta = 2$); deblurred image by (c) IDD-BM3D [41] (PSNR=25.00dB, FSIM=0.8606); (d) NCSR [42] (PSNR=24.90dB, FSIM=0.8588); (e) FPD [43] (PSNR=24.41dB, FSIM=0.8583); (f) MSEPLL [44] (PSNR=24.21dB, FSIM=0.8403); (g) GSR-NNM (PSNR=24.24dB, FSIM=0.8422); (h) GSR-WNNM (PSNR= 25.71dB, FSIM= 0.8701).

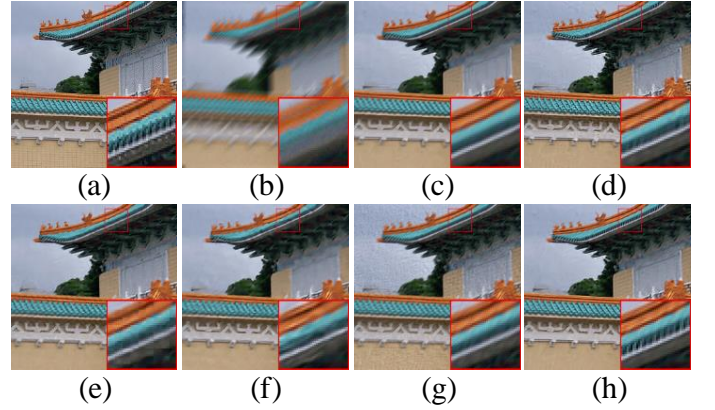


Fig. 3. Deblurring performance comparison on the *rampart* image. (a) Original image; (b) Noisy and blurred image (fspecial('gaussian', 25, 1.6), $\delta = 2$); deblurred image by (c) IDD-BM3D [41] (PSNR=26.18dB, FSIM=0.8529); (d) NCSR [42] (PSNR=26.21dB, FSIM=0.8674); (e) FPD [43] (PSNR=26.10dB, FSIM=0.8664); (f) MSEPLL [44] (PSNR=25.62dB, FSIM=0.8380); (g) GSR-NNM (PSNR=25.22dB, FSIM=0.8371); (h) GSR-WNNM (PSNR= 27.19dB, FSIM= 0.8872).

B. Image Inpainting

In this subsection, two interesting examples of image inpainting with different masks are conducted, i.e., image inpainting from partial random samples and text inlaid sample. The parameters are set as follows. $\varrho = 0.35$, $\epsilon = 0.35$ and $\rho = 0.1$. The size of searching window $R \times R$ is set to be 20×20 and searching matched patches $k = 60$. The size of each patch $\sqrt{m} \times \sqrt{m}$ is set to be 8×8 and 10×10 for partial random samples and text inlaid sampled, respectively.

We have compared the GSR-WNNM based image inpainting against five other competing approaches, including BPFA [45], IPPO [46], JSM [47], Aloha [48] and GSR-NNM. As can be seen from Table III, GSR-WNNM achieves the excellent competing performance of 8 color images to other leading methods. The visual comparisons of the image inpainting

methods are shown in Fig. 4 and Fig. 5, respectively. It can be seen that BPFA and GSR-NNM cannot reconstruct sharp edges and fine details. The IPPO, JSM and Aloha methods produce images with a much better visual quality than BPFA and GSR-NNM, but still suffer from some undesirable artifacts, such as the ringing effects. The proposed GSR-WNNM not only preserves sharper edges and finer details, but also eliminates the ringing effects.

C. Image Compressive Sensing

In this subsection, we report the experimental results of the proposed scheme based image CS recovery. we generate the CS measurements at the block level by utilizing a Gaussian random projection matrix to test images, i.e., the block-based CS recovery with block size of 32×32 . The parameters are

TABLE III
PSNR (dB) COMPARISONS FOR IMAGE INPAINTING.

Miss pixels	Method	Cowboy	Light	Mickey	Granny	Monk	Girl	Flower	Swamm
80%	BPFA [45]	24.93	19.23	24.53	24.71	35.06	24.80	27.30	27.93
	IPPO [46]	25.38	21.49	26.33	25.60	35.66	25.31	27.70	29.10
	JSM [47]	25.40	20.23	26.09	25.33	34.90	25.18	27.41	28.25
	Aloha [48]	25.06	21.50	25.33	25.54	35.51	25.16	27.49	28.63
	GSR-NNM	25.12	21.58	25.98	25.15	33.25	24.90	27.05	27.27
	GSR-WNNM	25.63	21.87	26.66	25.73	36.77	25.73	27.94	29.68
70%	BPFA [45]	26.76	21.58	26.16	26.62	37.43	26.86	28.92	29.65
	IPPO [46]	27.40	23.47	28.59	27.44	37.87	27.43	29.20	31.14
	JSM [47]	27.11	23.12	28.25	27.34	37.32	27.20	29.06	30.31
	Aloha [48]	27.24	23.17	27.11	27.43	38.00	27.08	29.02	30.78
	GSR-NNM	27.11	23.81	27.95	27.18	34.68	26.73	28.40	28.72
	GSR-WNNM	27.79	23.89	29.16	28.07	39.47	28.09	30.00	31.63
60%	BPFA [45]	28.42	23.65	27.83	28.63	39.38	28.75	30.61	31.60
	IPPO [46]	29.58	25.13	30.76	29.41	40.04	29.32	30.81	32.89
	JSM [47]	28.89	24.83	29.85	29.09	39.51	29.01	30.52	32.10
	Aloha [48]	28.92	24.47	28.59	29.51	40.30	28.91	30.72	32.20
	GSR-NNM	28.80	25.07	29.57	28.89	36.08	28.42	29.57	30.80
	GSR-WNNM	29.91	25.44	31.44	30.42	41.78	30.16	32.04	33.55
50%	BPFA [45]	30.21	25.71	29.43	30.68	41.77	30.58	32.55	33.32
	IPPO [46]	31.30	26.70	32.74	31.17	41.79	31.05	32.49	34.55
	JSM [47]	30.75	26.48	31.96	30.75	41.45	30.68	32.04	33.94
	Aloha [48]	30.46	25.84	30.33	31.24	42.65	30.59	32.40	33.85
	GSR-NNM	30.40	26.54	31.64	30.60	36.55	30.09	30.07	32.82
	GSR-WNNM	31.89	27.37	33.98	32.38	43.84	32.16	33.83	35.48
Inlay text	BPFA [45]	31.13	28.60	31.70	31.76	42.82	31.28	34.35	34.73
	IPPO [46]	32.61	29.92	34.04	33.01	44.21	32.65	35.15	36.93
	JSM [47]	32.42	29.65	32.99	32.40	42.70	32.20	34.59	36.56
	Aloha [48]	30.94	28.38	30.49	31.91	42.44	30.84	33.23	35.17
	GSR-NNM	32.16	29.59	32.75	32.25	40.91	31.88	34.17	35.64
	GSR-WNNM	33.18	30.44	35.02	33.58	45.33	33.20	35.73	37.30

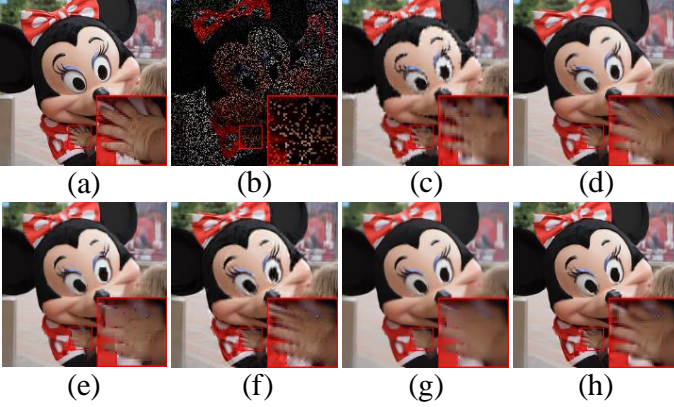


Fig. 4. Inpainting performance comparison on the *Mickey* image. (a) Original image; (b) Degraded image with 80% missing sample; Restoration results by (c) BPFA [45] (PSNR= 24.53dB, FSIM=0.8696); (d) IPPO [46] (PSNR=26.33dB, FSIM=0.9099); (e) JSM [47] (PSNR=26.09dB, FSIM=0.9060); (f) Aloha [48] (PSNR=25.33dB, FSIM=0.8770); (g) GSR-NNM (PSNR= 25.98dB, FSIM=0.8722); (h) GSR-WNNM (PSNR=**26.66dB**, FSIM=**0.9215**).



Fig. 5. Inpainting performance comparison on the *Girl* image. (a) Original image; (b) Degraded image with 80% missing sample; Restoration results by (c) BPFA [45] (PSNR= 24.80dB, FSIM=0.8765); (d) IPPO [46] (PSNR=25.31dB, FSIM=0.8914); (e) JSM [47] (PSNR=25.18dB, FSIM=0.8871); (f) Aloha [48] (PSNR=25.16dB, FSIM=0.8832); (g) GSR-NNM (PSNR= 24.90dB, FSIM=0.8398); (h) GSR-WNNM (PSNR=**25.73dB**, FSIM=**0.9123**).

set as follows. The size of searching window $R \times R$ is set to be 20×20 and searching matched patches $k = 60$. $\rho = 0.03$ for 0.1N measurements, and $\rho=0.1$ for other measurements. ϱ and $\epsilon = 0.35$. The size of each patch $\sqrt{m} \times \sqrt{m}$ is set to be 6×6 .

To verify the performance of the GSR-WNNM, we have compared it with some competitive CS recovery methods including the BCS [49], BM3D-CS [50], ADS-CS [51], SGSR [52], MRK [53] and GSR-NNM. The PSNR results of 8 gray

images are shown in Table IV. It can be seen that GSR-WNNM outperforms the other methods over different numbers of CS measurements. The average gain of GSR-WNNM over BCS, BM3D-CS, ADS-CS, SGSR, MRK and GSR-NNM can be as much as 7.21dB, 3.05dB, 1.40dB, 2.03dB, 2.23dB and 3.81dB, respectively. Some recovered images are presented in Fig. 6 and Fig. 7, respectively. It can be seen that BCS generates the worst perceptual result. The BM3D-CS, ADS-CS, SGSR, MRK, and GSR-NNM methods can obtain much better visual quality than BCS method, but still suffer from

TABLE IV
PSNR COMPARISONS FOR IMAGE CS RECOVERY.

Ratio	Method	boats	Fence	foreman	House	Leaves	Monarch	plants	straw
0.1	BCS [49]	24.54	19.52	29.73	26.99	18.55	21.96	27.39	19.19
	BM3D-CS [50]	25.40	17.63	32.66	32.50	18.93	23.23	28.27	18.10
	ADS-CS [51]	28.30	24.24	35.02	33.39	21.24	26.07	31.22	20.24
	SGSR [52]	27.71	25.52	34.88	32.77	22.22	24.27	30.16	20.20
	MRK [53]	28.32	20.67	35.29	32.43	22.05	26.97	31.72	20.36
	GSR-NNM	26.41	25.77	33.20	30.94	24.07	25.32	29.19	20.48
	GSR-WNNM	28.76	26.97	36.12	34.06	25.89	27.42	32.37	21.02
0.2	BCS [49]	27.05	21.57	32.82	30.54	21.12	25.21	30.67	20.69
	BM3D-CS [50]	31.01	22.57	37.87	35.04	28.14	30.37	34.98	20.04
	ADS-CS [51]	33.15	28.37	37.84	35.76	27.88	31.50	35.45	23.75
	SGSR [52]	32.41	29.38	36.98	35.81	28.74	28.75	34.65	24.40
	MRK [53]	32.38	22.20	38.62	36.36	27.75	31.28	35.99	23.02
	GSR-NNM	30.23	27.96	35.59	33.96	28.50	28.86	31.99	23.65
	GSR-WNNM	34.02	30.19	38.90	37.07	31.64	32.19	37.17	24.82
0.3	BCS [49]	28.91	23.24	35.13	32.85	23.16	27.55	32.81	22.19
	BM3D-CS [50]	34.04	30.68	40.48	36.84	32.52	34.69	38.30	22.37
	ADS-CS [51]	36.35	31.29	39.79	38.21	32.55	35.02	38.45	26.58
	SGSR [52]	35.21	31.41	38.47	37.37	32.98	31.98	37.20	27.26
	MRK [53]	34.97	24.44	40.72	38.35	32.37	34.25	39.06	25.52
	GSR-NNM	32.37	29.49	36.80	35.17	29.37	30.90	33.41	25.50
	GSR-WNNM	37.11	32.50	41.10	39.07	35.65	35.37	39.98	27.84
0.4	BCS [49]	30.56	24.81	36.98	34.65	25.07	29.59	34.77	23.71
	BM3D-CS [50]	36.71	33.83	42.40	38.08	36.01	37.59	41.17	24.38
	ADS-CS [51]	38.79	34.02	41.60	40.30	35.94	37.77	40.77	28.80
	SGSR [52]	37.41	33.20	39.85	38.99	35.83	34.65	39.24	29.45
	MRK [53]	37.20	26.63	42.40	40.04	35.53	36.66	41.64	27.69
	GSR-NNM	33.85	30.82	37.50	36.18	31.14	31.70	34.97	27.06
	GSR-WNNM	39.39	34.50	42.88	40.82	38.85	38.13	42.24	30.30

some undesirable artifacts or over-smooth phenomena, such as ring effects and loss of some fine image details. By contrast, GSR-WNNM not only removes most of the visual artifacts, but also preserves large-scale sharp edges and small-scale fine image details more effectively in comparison with other competing methods.

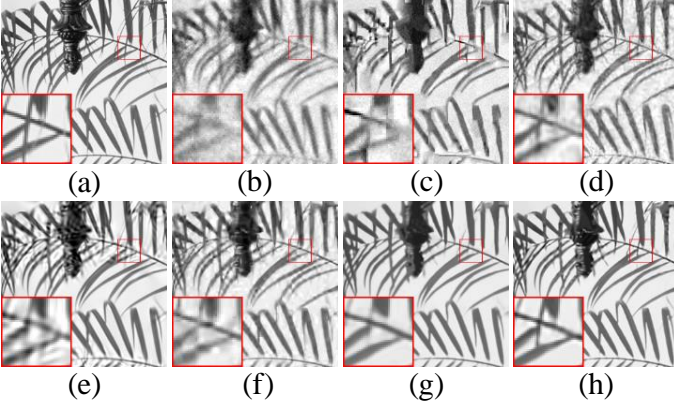


Fig. 6. CS recovered *Leaves* images with $0.1N$ measurements. (a) original image; (b) BCS [49] (PSNR=18.55dB, FSIM=0.6827); (c) BM3D-CS [50] (PSNR=18.93dB, FSIM=0.7259); (d) ADS-CS [51] (PSNR=21.24dB, FSIM=0.7671); (e) SGSR [52] (PSNR=22.22dB, FSIM=0.8356); (f) MRK [53] (PSNR=22.05dB, FSIM=0.8118); (g) GSR-NNM (PSNR=24.07dB, FSIM=0.8821); (h) GSR-WNNM (PSNR= **25.89dB**, FSIM=**0.9168**).

According to above analysis, it can be seen that GSR-WNNM significantly outperforms GSR-NNM. Therefore, the above analysis are indirect evidence that WNNM is more accurate than NNM.

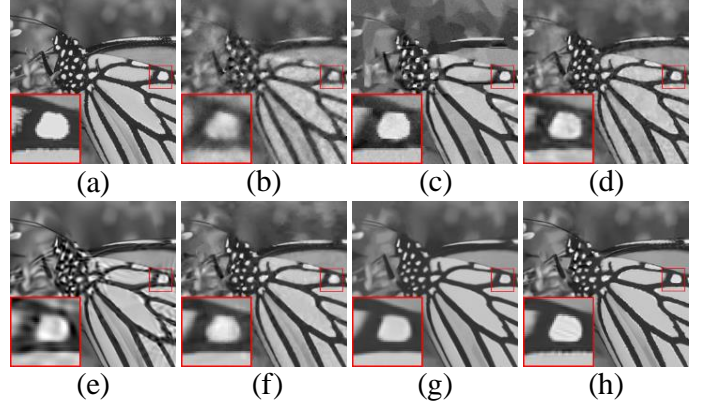


Fig. 7. CS recovered *Monarch* images with $0.1N$ measurements. (a) original image; (b) BCS [49] (PSNR=21.96dB, FSIM=0.7868); (c) BM3D-CS [50] (PSNR=23.23dB, FSIM=0.8093); (d) ADS-CS [51] (PSNR=26.07dB, FSIM=0.8566); (e) SGSR [52] (PSNR=24.27dB, FSIM=0.8371); (f) MRK [53] (PSNR=26.97dB, FSIM=0.8874); (g) GSR-NNM (PSNR=25.32dB, FSIM=0.8652); (h) GSR-WNNM (PSNR= **27.42dB**, FSIM=**0.9076**).

D. Effect of the number of the best matched patches

We have discussed how to select the best matching patch numbers k for the performance of the proposed approach. Specifically, to investigate the sensitivity of our approach against k , two experiments are conducted with respect to different k , ranging from 20 to 200, in the case of image CS recovery and image deblurring, respectively. The results with different k are shown in Fig. 8. It can be seen that all the curves are almost flat, showing the performance of GSR-WNNM is insensitive to k . The best performance of each case is usually achieved with k in the range [40,80]. Therefore, in

this paper k is empirically set to be 60.

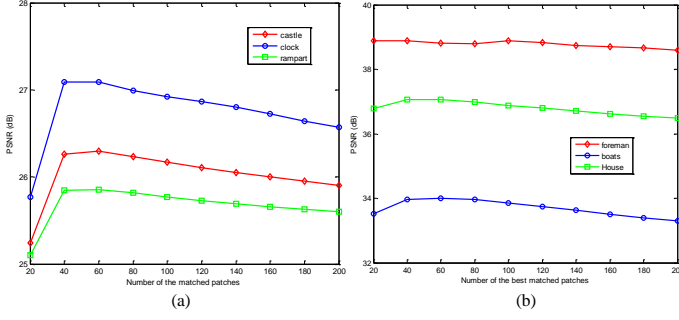


Fig. 8. Performance comparison with different matched patch numbers k for image CS recovery and image inpainting. (a) PSNR results achieved by different k in the case of the image deblurring with 9×9 uniform blur kernel. (b) PSNR results achieved by different k in the case of the image CS recovery with $0.2N$ measurements.

E. Comparison of the noise level for different methods

Two experiments are conducted to demonstrate the robustness of the proposed GSR-WNNM against noise in the case of image deblurring and CS recovery. A significant amount of additive gaussian noise is added to color image *Corner* with 9×9 uniform blur kernel and gray image *House* with $0.1N$ CS measurements, respectively. The standard derivations of additive noise are varied to generate the signal-to-noise-ratio (SNR) includes 10dB, 15dB, 20dB, 25dB, 30dB, 35dB and 40dB. The PSNR comparison of the reconstructed images is shown in Fig. 9. It can be seen that the proposed GSR-WNNM approach achieves the best performance.

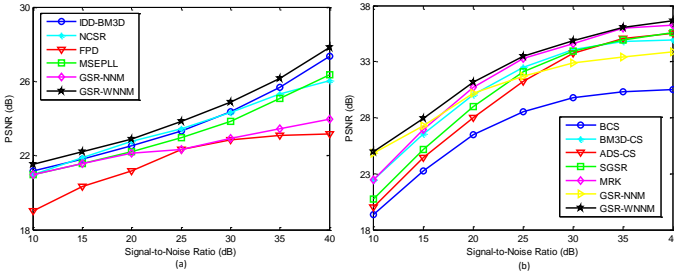


Fig. 9. PSNR of the different methods from noisy levels. (a) PSNR results versus SNR with 9×9 uniform kernel for image *Corner*. (b) PSNR results versus SNR with $0.1N$ measurements for image *House*.

F. Comparison Between ADMM and IST

In this subsection, another classical optimization approach: iterative shrinkage/thresholding (IST) [32] is exploited to solve our proposed scheme for CS image reconstruction. We will make a comparison between ADMM and IST with ratio = 0.2 and ratio = 0.3 for two image *foreman* and *House* as examples, respectively. Fig. 10 shows their progression curves of the PSNR (dB) results achieved by ADMM and IST, respectively. It can be seen that ADMM algorithm is more fast efficient and effective to solve the proposed scheme than IST algorithm.

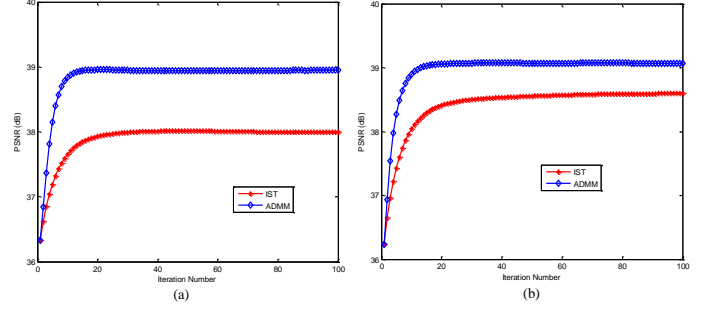


Fig. 10. Comparison between ADMM and IST. (a) PSNR results achieved by ADMM and IST with ratio = 0.2 for image *foreman*. (b) PSNR results achieved by ADMM and IST with ratio = 0.3 for image *House*.

G. Convergence

Fig. 11 illustrates the convergence analysis of the proposed GSR-WNNM. It shows the curves of the PSNR values versus the iteration numbers for image CS with $0.1N$ measurements as well as image deblurring with 9×9 uniform kernel and $\delta = 2$, respectively. It can be seen that with the increase of the iteration number, the PSNR curves of the reconstructed images gradually increase and become flat and stable. Therefore, the proposed GSR-WNNM has a good convergence.

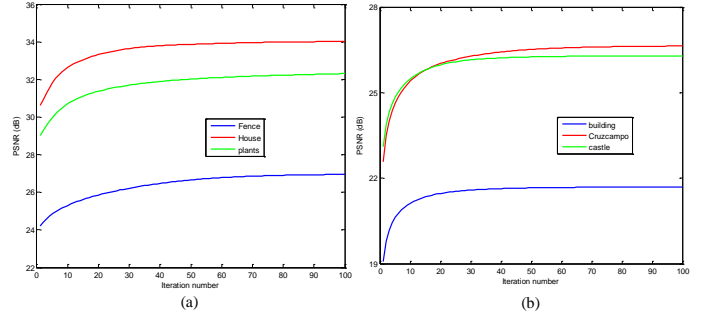


Fig. 11. Convergence analysis of the proposed GSR-WNNM method. (a) PSNR results versus iteration number for image CS recovery with $0.1N$ measurements. (b) PSNR results versus iteration number for image deblurring with 9×9 uniform blur and $\delta = 2$.

VI. CONCLUSION

This paper analyzed the weighted nuclear norm minimization (WNNM) and nuclear norm minimization (NNM) based on group sparse representation (GSR). We designed an adaptive dictionary for each group to connect the rank minimization and GSR models. We proved that the equivalence of the rank minimization and GSR models. Based on that conclusion, we showed mathematically that WNNM is more accurate than NNM. To make the proposed model tractable and robust, the alternative direction multiplier method (ADMM) framework was adopted to solve the proposed model. Experimental results on three low-level vision applications, i.e., image deblurring, image inpainting and image CS recovery, have demonstrated that the proposed scheme outperforms many state-of-the-art methods.

APPENDIX A
PROOF OF THE THEOREM 3

Theorem 3. For $0 \leq w_1 \leq \dots \leq w_{n_0}$ and \mathbf{Y} , $n_0 = \min(m, k)$, the singular value shrinkage operator Eq. (8) satisfies Eq. (7).

Proof. For fixed weights \mathbf{W} , $h_0(\mathbf{X}) = \frac{1}{2} \|\mathbf{Y} - \mathbf{X}\|_F^2 + \|\mathbf{X}\|_{\mathbf{W},*}$, $\hat{\mathbf{X}}$ minimizes h_0 if and only if it satisfies the following optimal condition,

$$\mathbf{0} \in \hat{\mathbf{X}} - \mathbf{Y} + \partial \|\hat{\mathbf{X}}\|_{\mathbf{W},*} \quad (35)$$

where $\partial \|\hat{\mathbf{X}}\|_{\mathbf{W},*}$ is the set of subgradients of the weighted nuclear norm. Let matrix $\mathbf{X} \in \mathbb{R}^{m \times k}$ be an arbitrary matrix and its SVD be $\mathbf{U}\Sigma\mathbf{V}^T$. It is known from [30, 54] that the subgradient of $\|\mathbf{X}\|_{\mathbf{W},*}$ can be derived as

$$\begin{aligned} \partial \|\mathbf{X}\|_{\mathbf{W},*} &= \{\mathbf{U}\mathbf{W}_r\mathbf{V}^T + \mathbf{Z} : \mathbf{Z} \in \mathbb{R}^{m \times k}, \mathbf{U}^T\mathbf{Z} = \mathbf{0}, \\ \mathbf{Z}\mathbf{V} &= \mathbf{0}, \sigma_j(\mathbf{Z}) \leq w_{r+j}, j = 1, \dots, n_0 - r\} \end{aligned} \quad (36)$$

where r is the rank of \mathbf{X} and \mathbf{W}_r is the diagonal matrix composed of the first r rows and r columns of the diagonal matrix $\text{diag}(\mathbf{W})$. Note that the sub-gradient conclusion in Eqs. (35) and (36) has been proved for convex problem [3]. Nonetheless, they are feasible for non-convex problem [55].

In order to show that $\hat{\mathbf{X}}$ obeys Eq. (36), the SVD of \mathbf{Y} can be rewritten as

$$\mathbf{Y} = \mathbf{U}_0 \Sigma_0 \mathbf{V}_0^T + \mathbf{U}_1 \Sigma_1 \mathbf{V}_1^T \quad (37)$$

where $\mathbf{U}_0, \mathbf{V}_0$ (resp. $\mathbf{U}_1, \mathbf{V}_1$) are the singular vectors associated with singular values greater than w_j (resp. smaller than or equal to w_j). With these notations, we have

$$\hat{\mathbf{X}} = \mathbf{U}_0(\Sigma_0 - \mathbf{W}_r)\mathbf{V}_0^T \quad (38)$$

Therefore,

$$\mathbf{Y} - \hat{\mathbf{X}} = \mathbf{U}_0 \mathbf{W}_r \mathbf{V}_0^T + \mathbf{Z} \quad (39)$$

where $\mathbf{Z} = \mathbf{U}_1 \Sigma_1 \mathbf{V}_1^T$, by definition, $\mathbf{U}_0^T \mathbf{Z} = \mathbf{0}, \mathbf{Z} \mathbf{V}_0 = \mathbf{0}$ and since the diagonal elements of Σ_1 are smaller than w_{j+r} , it is easy to verify that $\sigma_j \leq w_{r+j}, j = 1, 2, \dots, n_0 - r$. Thus, $\mathbf{Y} - \hat{\mathbf{X}} \in \partial \|\hat{\mathbf{X}}\|_{\mathbf{W},*}$, which concludes the proof. \square

APPENDIX B
PROOF OF THE LEMMA 2

Proof. Without considering the constraint, the optimization problem Eq. (13) can be rewritten as the following unconstrained form,

$$\min_{x_i \geq 0} \frac{1}{2} (x_i - a_i)^2 + w_i x_i \Leftrightarrow \min_{x_i \geq 0} \frac{1}{2} (x_i - (a_i - w_i))^2 \quad (40)$$

Thus, it can be easily derived that the global optimization solution of Eq. (40) is

$$\hat{x}_i = \max(a_i - w_i, 0), i = 1, 2, \dots, n. \quad (41)$$

As we have $a_1 \geq \dots \geq a_n \geq 0$ and the weights $0 \leq w_1 \leq \dots \leq w_n$, it can be seen that $\hat{x}_1 \geq \hat{x}_2 \geq \dots \geq \hat{x}_n$. Thus, $\hat{x}_{i=1,2,\dots,n}$ obeys the constraint of Eq. (13), and thus $\hat{x}_i = \max(a_i - w_i, 0)$ is the global solution of Eq. (13). \square

APPENDIX C
PROOF OF THE THEOREM 4

Proof. Since the adaptive dictionary \mathbf{D}_i is constructed by Eq. (10), and the unitary property of \mathbf{U}_i and \mathbf{V}_i , we have

$$\begin{aligned} \|\mathbf{Y}_i - \mathbf{X}_i\|_F^2 &= \|\mathbf{D}_i(\boldsymbol{\mu}_i - \boldsymbol{\alpha}_i)\|_F^2 = \|\mathbf{U}_i \text{diag}(\boldsymbol{\mu}_i - \boldsymbol{\alpha}_i) \mathbf{V}_i\|_F^2 \\ &= \text{trace}(\mathbf{U}_i \text{diag}(\boldsymbol{\mu}_i - \boldsymbol{\alpha}_i) \mathbf{V}_i \mathbf{V}_i^T \text{diag}(\boldsymbol{\mu}_i - \boldsymbol{\alpha}_i) \mathbf{U}_i^T) \\ &= \text{trace}(\mathbf{U}_i \text{diag}(\boldsymbol{\mu}_i - \boldsymbol{\alpha}_i) \text{diag}(\boldsymbol{\mu}_i - \boldsymbol{\alpha}_i) \mathbf{U}_i^T) \\ &= \text{trace}(\text{diag}(\boldsymbol{\mu}_i - \boldsymbol{\alpha}_i) \mathbf{U}_i \mathbf{U}_i^T \text{diag}(\boldsymbol{\mu}_i - \boldsymbol{\alpha}_i)) \\ &= \text{trace}(\text{diag}(\boldsymbol{\mu}_i - \boldsymbol{\alpha}_i) \text{diag}(\boldsymbol{\mu}_i - \boldsymbol{\alpha}_i)) \\ &= \|\boldsymbol{\mu}_i - \boldsymbol{\alpha}_i\|_2^2 \end{aligned} \quad (42)$$

APPENDIX D
PROOF OF THE PROPOSITION 2

Proposition 2. WNNM is more accurate than NNM under the adaptive dictionary \mathbf{D}_i .

Proof. On the basis of Theorem 4, we have

$$\begin{aligned} \boldsymbol{\alpha}_i &= \arg \min_{\boldsymbol{\alpha}_i} \frac{1}{2} \|\mathbf{Y}_i - \mathbf{D}_i \boldsymbol{\alpha}_i\|_F^2 + \lambda_i \|\boldsymbol{\alpha}_i\|_1 \\ &= \arg \min_{\boldsymbol{\alpha}_i} \frac{1}{2} \|\boldsymbol{\mu}_i - \boldsymbol{\alpha}_i\|_2^2 + \lambda_i \|\boldsymbol{\alpha}_i\|_1 \end{aligned} \quad (43)$$

Thus, based on Lemma 1, we have

$$\boldsymbol{\alpha}_i = \text{soft}(\boldsymbol{\mu}_i, \lambda_i) = \max(\text{abs}(\boldsymbol{\mu}_i) - \lambda_i, 0) \quad (44)$$

Obviously, according to Eqs. (9) and (10), we have

$$\begin{aligned} \hat{\mathbf{X}}_i &= \mathbf{D}_i \boldsymbol{\alpha}_i = \sum_{j=1}^{n_0} \text{soft}(\boldsymbol{\mu}_{i,j}, \lambda_i) \mathbf{d}_{i,j} \\ &= \sum_{j=1}^{n_0} \text{soft}(\boldsymbol{\mu}_{i,j}, \lambda_i) \mathbf{u}_{i,j} \mathbf{v}_{i,j}^T \\ &= \mathbf{U}_i \mathbf{S}_{\lambda_i}(\boldsymbol{\Sigma}_i) \mathbf{V}_i^T \end{aligned} \quad (45)$$

where $\boldsymbol{\mu}_{i,j}$ represents the j -th element of the i -th group sparse coefficient $\boldsymbol{\mu}_i$, and $\boldsymbol{\Sigma}_i$ is the singular value matrix of the i -th group \mathbf{Y}_i .

Thus, based on Theorem 1, we prove that the ℓ_1 -norm based GSR problem (Eq. (43)) is equivalent to the NNM problem (Eq. (5)).

Similarly, based on Theorem 4, for the weighted ℓ_1 norm-based group sparse representation problem, we have

$$\begin{aligned} \boldsymbol{\alpha}_i &= \arg \min_{\boldsymbol{\alpha}_i} \frac{1}{2} \|\mathbf{Y}_i - \mathbf{D}_i \boldsymbol{\alpha}_i\|_F^2 + \|\mathbf{w}_i \boldsymbol{\alpha}_i\|_1 \\ &= \arg \min_{\boldsymbol{\alpha}_i} \frac{1}{2} \|\boldsymbol{\mu}_i - \boldsymbol{\alpha}_i\|_2^2 + \|\mathbf{w}_i \boldsymbol{\alpha}_i\|_1 \end{aligned} \quad (46)$$

Thus, based on Lemma 2, we have

$$\boldsymbol{\alpha}_i = \text{soft}(\boldsymbol{\mu}_i, \mathbf{w}_i) = \max(\boldsymbol{\mu}_i - \mathbf{w}_i, 0) \quad (47)$$

Based on Eqs. (9) and (10), we have

$$\begin{aligned} \hat{\mathbf{X}}_i &= \mathbf{D}_i \boldsymbol{\alpha}_i = \sum_{j=1}^{n_0} \text{soft}(\boldsymbol{\mu}_{i,j}, \mathbf{w}_i) \mathbf{d}_{i,j} \\ &= \sum_{j=1}^{n_0} \text{soft}(\boldsymbol{\mu}_{i,j}, \mathbf{w}_i) \mathbf{u}_{i,j} \mathbf{v}_{i,j}^T \\ &= \mathbf{U}_i \mathbf{S}_{\mathbf{w}_i}(\boldsymbol{\Sigma}_i) \mathbf{V}_i^T \end{aligned} \quad (48)$$

Therefore, based on *Theorem 3*, we prove that the weighted ℓ_1 norm-based GSR problem (Eq. (46)) is equivalent to the WNNM problem (Eq. (7)).

Proposition 1 has showed that the weighted ℓ_1 norm has much more sparsity encouraging than the ℓ_1 norm [28]. Meanwhile, based on group sparse representation, we have proven that WNNM, NNM are equivalent to the weighted ℓ_1 norm minimization and ℓ_1 norm minimization, respectively. Therefore, we prove that WNNM is more accurate than NNM. \square

APPENDIX E

PROOF OF THE THEOREM 5

Proof. Owing to the assumption that $\mathbf{e}(\mathbf{j})$ follows an independent zero mean distribution with variance δ^2 , namely, $\mathbf{E}[\mathbf{e}(\mathbf{j})] = 0$ and $\mathbf{Var}[\mathbf{e}(\mathbf{j})] = \delta^2$. Thus, it can be deduced that each $\mathbf{e}(\mathbf{j})^2$ is also independent, and the meaning of each $\mathbf{e}(\mathbf{j})^2$ is:

$$\mathbf{E}[\mathbf{e}(\mathbf{j})^2] = \mathbf{Var}[\mathbf{e}(\mathbf{j})] + [\mathbf{E}[\mathbf{e}(\mathbf{j})]]^2 = \delta^2, j = 1, 2, \dots, N \quad (49)$$

By invoking the *law of Large numbers* in probability theory, for any $\varepsilon > 0$, it leads to $\lim_{N \rightarrow \infty} \mathbf{P}\{|\frac{1}{N} \sum_{j=1}^N \mathbf{e}(\mathbf{j})^2 - \delta^2| < \frac{\varepsilon}{2}\} = 1$, namely,

$$\lim_{N \rightarrow \infty} \mathbf{P}\{|\frac{1}{N} \|\mathbf{X} - \mathbf{L}\|_2^2 - \delta^2| < \frac{\varepsilon}{2}\} = 1 \quad (50)$$

Next, we denote the concatenation of all the groups \mathbf{X}_i and \mathbf{L}_i , $i = 1, 2, \dots, n$, by \mathbf{X} and \mathbf{L} , respectively. Meanwhile, we denote the error of each element of $\mathbf{X} - \mathbf{L}$ by $\mathbf{e}(k)$, $k = 1, 2, \dots, K$. We have also denote $\mathbf{e}(k)$ following an independent zero mean distribution with variance δ^2 .

Therefore, the same process applied to $\mathbf{e}(k)^2$ yields $\lim_{N \rightarrow \infty} \mathbf{P}\{|\frac{1}{N} \sum_{k=1}^N \mathbf{e}(k)^2 - \delta^2| < \frac{\varepsilon}{2}\} = 1$, i.e.,

$$\lim_{N \rightarrow \infty} \mathbf{P}\{|\frac{1}{N} \sum_{i=1}^n \|\mathbf{X}_i - \mathbf{L}_i\|_2^2 - \delta^2| < \frac{\varepsilon}{2}\} = 1 \quad (51)$$

Obviously, considering Eqs. (50) and (51) together, we can prove Eq. (28). \square

REFERENCES

- [1] Srebro N, Salakhutdinov R R. Collaborative filtering in a non-uniform world: Learning with the weighted trace norm[C]//Advances in Neural Information Processing Systems. 2010: 2056-2064.
- [2] Li X, Cui G, Dong Y. Graph regularized non-negative low-rank matrix factorization for image clustering[J]. IEEE Transactions on Cybernetics, 2016.
- [3] Cai J F, Cands E J, Shen Z. A singular value thresholding algorithm for matrix completion[J]. SIAM Journal on Optimization, 2010, 20(4): 1956-1982.
- [4] Fang X, Xu Y, Li X, et al. Robust semi-supervised subspace clustering via non-negative low-rank representation[J]. IEEE transactions on cybernetics, 2016, 46(8): 1828-1838.
- [5] Zheng Y, Liu G, Sugimoto S, et al. Practical low-rank matrix approximation under robust ℓ_1 -norm[C]//Computer Vision and Pattern Recognition (CVPR), 2012 IEEE Conference on. IEEE, 2012: 1410-1417.
- [6] Wen Z, Hou B, Jiao L. Discriminative Dictionary Learning With Two-Level Low Rank and Group Sparse Decomposition for Image Classification[J]. IEEE transactions on cybernetics, 2016.
- [7] Wright J, Ganesh A, Rao S, et al. Robust principal component analysis: Exact recovery of corrupted low-rank matrices via convex optimization[C]//Advances in neural information processing systems. 2009: 2080-2088.
- [8] Mu Y, Dong J, Yuan X, et al. Accelerated low-rank visual recovery by random projection[C]//Computer Vision and Pattern Recognition (CVPR), 2011 IEEE Conference on. IEEE, 2011: 2609-2616.
- [9] Peng Y, Ganesh A, Wright J, et al. RASL: Robust alignment by sparse and low-rank decomposition for linearly correlated images[J]. IEEE Transactions on Pattern Analysis and Machine Intelligence, 2012, 34(11): 2233-2246.
- [10] Ji H, Huang S, Shen Z, et al. Robust video restoration by joint sparse and low rank matrix approximation[J]. SIAM Journal on Imaging Sciences, 2011, 4(4): 1122-1142.
- [11] Cands E J, Li X, Ma Y, et al. Robust principal component analysis?[J]. Journal of the ACM (JACM), 2011, 58(3): 11.
- [12] Eriksson A, Van Den Hengel A. Efficient computation of robust low-rank matrix approximations in the presence of missing data using the ℓ_1 -norm[C]//Computer Vision and Pattern Recognition (CVPR), 2010 IEEE Conference on. IEEE, 2010: 771-778.
- [13] Liu G, Lin Z, Yan S, et al. Robust recovery of subspace structures by low-rank representation[J]. IEEE Transactions on Pattern Analysis and Machine Intelligence, 2013, 35(1): 171-184.
- [14] Lu C Y, Min H, Zhao Z Q, et al. Robust and efficient subspace segmentation via least squares regression[J]. Computer VisionCECCV 2012, 2012: 347-360.
- [15] Gu S, Zhang L, Zuo W, et al. Weighted nuclear norm minimization with application to image denoising[C]//Proceedings of the IEEE Conference on Computer Vision and Pattern Recognition. 2014: 2862-2869.
- [16] Lu C, Tang J, Yan S, et al. Generalized nonconvex nonsmooth low-rank minimization[C]//Proceedings of the IEEE Conference on Computer Vision and Pattern Recognition. 2014: 4130-4137.
- [17] Gu S, Xie Q, Meng D, et al. Weighted nuclear norm minimization and its applications to low level vision[J]. International Journal of Computer Vision, 2016: 1-26.
- [18] Lu C, Tang J, Yan S, et al. Nonconvex nonsmooth low rank minimization via iteratively reweighted nuclear norm[J]. IEEE Transactions on Image Processing, 2016, 25(2): 829-839.
- [19] Sadigh D, Ohlsson H, Sastry S S, et al. Robust subspace system identification via weighted nuclear norm optimization[J]. IFAC Proceedings Volumes, 2014, 47(3): 9510-9515.
- [20] Chen F, Zhang L, Yu H. External patch prior guided internal clustering for image denoising[C]//Proceedings of the IEEE International Conference on Computer Vision. 2015: 603-611.
- [21] Aharon M, Elad M, Bruckstein A. k -SVD: An algorithm for designing overcomplete dictionaries for sparse representation[J]. IEEE Transactions on signal processing, 2006, 54(11): 4311-4322.
- [22] Elad M, Aharon M. Image denoising via sparse and redundant representations over learned dictionaries[J]. IEEE Transactions on Image processing, 2006, 15(12): 3736-3745.
- [23] Zhang Q, Li B. Discriminative K-SVD for dictionary learning in face recognition[C]//Computer Vision and Pattern Recognition (CVPR), 2010 IEEE Conference on. IEEE, 2010: 2691-2698.
- [24] Mairal J, Elad M, Sapiro G. Sparse representation for color image restoration[J]. IEEE Transactions on image processing, 2008, 17(1): 53-69.
- [25] Mairal J, Bach F, Ponce J, et al. Non-local sparse models for image restoration[C]//Computer Vision, 2009 IEEE 12th International Conference on. IEEE, 2009: 2272-2279.
- [26] Zhang J, Zhao D, Gao W. Group-based sparse representation for image restoration[J]. IEEE Transactions on Image Processing, 2014, 23(8): 3336-3351.
- [27] Zha Z, Liu X, Huang X, et al. Analyzing the group sparsity

- based on the rank minimization methods[J]. arXiv preprint arXiv:1611.08983, 2016.
- [28] Candes E J, Wakin M B, Boyd S P. Enhancing sparsity by reweighted ℓ_1 minimization[J]. *Journal of Fourier analysis and applications*, 2008, 14(5): 877-905.
 - [29] Fazel M. Matrix rank minimization with applications[D]. PhD thesis, Stanford University, 2002.
 - [30] Candes E, Recht B. Exact matrix completion via convex optimization[J]. *Communications of the ACM*, 2012, 55(6): 111-119.
 - [31] Li C, Yin W, Zhang Y. Users guide for TVAL3: TV minimization by augmented lagrangian and alternating direction algorithms[J]. *CAAM report*, 2009, 20: 46-47.
 - [32] Beck A, Teboulle M. Fast gradient-based algorithms for constrained total variation image denoising and deblurring problems[J]. *IEEE Transactions on Image Processing*, 2009, 18(11): 2419-2434.
 - [33] Boyd S, Parikh N, Chu E, et al. Distributed optimization and statistical learning via the alternating direction method of multipliers[J]. *Foundations and Trends in Machine Learning*, 2011, 3(1): 1-122.
 - [34] Zhao C, Zhang J, Ma S, et al. Nonconvex Lp Nuclear Norm based ADMM Framework for Compressed Sensing[C]//Data Compression Conference (DCC), 2016. IEEE, 2016: 161-170.
 - [35] Chartrand R, Wohlberg B. A nonconvex ADMM algorithm for group sparsity with sparse groups[C]//Acoustics, Speech and Signal Processing (ICASSP), 2013 IEEE International Conference on. IEEE, 2013: 6009-6013.
 - [36] Zha Z, Zhang X, Wu Y, et al. Non-Convex Weighted Schatten p-Norm Minimization based ADMM Framework for Image Restoration[J]. arXiv preprint arXiv:1704.07056, 2017.
 - [37] Afonso M V, Bioucas-Dias J M, Figueiredo M A T. Fast image recovery using variable splitting and constrained optimization[J]. *IEEE Transactions on Image Processing*, 2010, 19(9): 2345-2356.
 - [38] Avriel M. Nonlinear programming: analysis and methods[M]. Courier Corporation, 2003.
 - [39] Chang S G, Yu B, Vetterli M. Adaptive wavelet thresholding for image denoising and compression[J]. *IEEE Transactions on image processing*, 2000, 9(9): 1532-1546.
 - [40] Zhang L, Zhang L, Mou X, et al. FSIM: A feature similarity index for image quality assessment[J]. *IEEE transactions on Image Processing*, 2011, 20(8): 2378-2386.
 - [41] Danielyan A, Katkovnik V, Egiazarian K. BM3D frames and variational image deblurring[J]. *IEEE Transactions on Image Processing*, 2012, 21(4): 1715-1728.
 - [42] Dong W, Zhang L, Shi G, et al. Nonlocally centralized sparse representation for image restoration[J]. *IEEE Transactions on Image Processing*, 2013, 22(4): 1620-1630.
 - [43] Xu Y, Yin W. A fast patch-dictionary method for whole image recovery[J]. arXiv preprint arXiv:1408.3740, 2014.
 - [44] Pappyan V, Elad M. Multi-scale patch-based image restoration[J]. *IEEE Transactions on image processing*, 2016, 25(1): 249-261.
 - [45] Zhou M, Chen H, Ren L, et al. Non-parametric Bayesian dictionary learning for sparse image representations[C]//Advances in neural information processing systems. 2009: 2295-2303.
 - [46] Ram I, Elad M, Cohen I. Image processing using smooth ordering of its patches[J]. *IEEE transactions on image processing*, 2013, 22(7): 2764-2774.
 - [47] Zhang J, Zhao D, Xiong R, et al. Image restoration using joint statistical modeling in a space-transform domain[J]. *IEEE Transactions on Circuits and Systems for Video Technology*, 2014, 24(6): 915-928.
 - [48] Jin K H, Ye J C. Annihilating filter-based low-rank Hankel matrix approach for image inpainting[J]. *IEEE Transactions on Image Processing*, 2015, 24(11): 3498-3511.
 - [49] Mun S, Fowler J E. Block compressed sensing of images using directional transforms[C]//Image Processing (ICIP), 2009 16th IEEE International Conference on. IEEE, 2009: 3021-3024.
 - [50] Egiazarian K, Foi A, Katkovnik V. Compressed sensing image reconstruction via recursive spatially adaptive filtering[C]//Image Processing, 2007. ICIP 2007. IEEE International Conference on. IEEE, 2007, 1: I-549-I-552.
 - [51] Dong W, Shi G, Li X, et al. Image reconstruction with locally adaptive sparsity and nonlocal robust regularization[J]. *Signal Processing: Image Communication*, 2012, 27(10): 1109-1122.
 - [52] Zhang J, Zhao D, Jiang F, et al. Structural group sparse representation for image compressive sensing recovery[C]//Data Compression Conference (DCC), 2013. IEEE, 2013: 331-340.
 - [53] Canh T N, Dinh K Q, Jeon B. Multi-scale/multi-resolution Kronecker compressive imaging[C]//Image Processing (ICIP), 2015 IEEE International Conference on. IEEE, 2015: 2700-2704.
 - [54] Lewis A S. The convex analysis of unitarily invariant matrix functions[J]. *Journal of Convex Analysis*, 1995, 2(1): 173-183.
 - [55] Dong W, Shi G, Li X, et al. Compressive sensing via non-local low-rank regularization[J]. *IEEE Transactions on Image Processing*, 2014, 23(8): 3618-3632.